Three-spin solid effect and the spin diffusion barrier in amorphous solids

Tan, Kong Ooi; Mardini, Michael; Yang, Chen; Ardenkjær-Larsen, Jan Henrik; Griffin, Robert G.

Published in:
Science Advances

Link to article, DOI:
10.1126/sciadv.aax2743

Publication date:
2019

Document Version
Publisher's PDF, also known as Version of record

CHEMICAL PHYSICS

Three-spin solid effect and the spin diffusion barrier in amorphous solids

Kong Ooi Tan[1], Michael Mardini[1], Chen Yang[1]*, Jan Henrik Ardenkjær-Larsen[2,3], Robert G. Griffin[1†]

Dynamic nuclear polarization (DNP) has evolved as the method of choice to enhance NMR signal intensities and to address a variety of otherwise inaccessible chemical, biological and physical questions. Despite its success, there is no detailed understanding of how the large electron polarization is transferred to the surrounding nuclei or where these nuclei are located relative to the polarizing agent. To address these questions we perform an analysis of the three-spin solid effect, and show that it is exquisitely sensitive to the electron-nuclear distances. We exploit this feature and determine that the size of the spin diffusion barrier surrounding the trityl radical in a glassy glycerol–water matrix is <6 Å, and that the protons involved in the initial transfer step are on the trityl molecule. ^{1}H ENDOR experiments indicate that polarization is then transferred in a second step to glycerol molecules in intimate contact with the trityl.

INTRODUCTION

Microwave-driven dynamic nuclear polarization (DNP) (*1*, *2*) is a well-established method used to enhance nuclear magnetic resonance (NMR) signal intensities by transferring polarization from unpaired electrons to nearby nuclei. Subsequently, this polarization is transferred to more distant nuclei and polarizes the entire sample via spin diffusion (*3*). There are four different mechanisms that use continuous wave microwave irradiation to drive the polarization transfer in DNP, namely, the Overhauser effect, cross effect (CE), solid effect (SE), and thermal mixing (*4*–*7*). In general, these mechanisms yield large signal enhancements (≥100) leading to experimental time savings of $\geq 10^4$. However, in an amorphous, glassy, glycerol-water matrix, which is a medium frequently used for DNP, the mechanism by which the electron polarization moves from the polarizing agent to the nuclei of the solvent or target molecule is not known. Here, we use our recent experimental observation and theoretical analysis of the three-spin solid effect (TSSE), together with ^{1}H electron nuclear double-resonance (^{1}H ENDOR) and ELDOR-detected NMR (EDNMR) spectra, to address this question. We find that, for the case of trityl radical dispersed in glycerol-water solvents, the ^{1}H's polarized in the initial step of DNP are less than a few angstroms from the electron and reside on the trityl molecule. Furthermore, ^{1}H ENDOR experiments indicate that the electron polarization is first transferred to the intramolecular ^{1}H's on the trityl radical and then via spin diffusion to glycerol molecules in intimate contact with the trityl.

The SE mechanism, on which this paper is largely based, was first discussed theoretically by Jeffries (*8*) and later demonstrated experimentally by Abragam and Proctor (*4*). In an SE experiment, microwave irradiation is applied at an electron offset frequency that matches the nuclear Larmor frequency ($\Omega_S = \pm\omega_{0I}$) to drive the polarization transfer via either a double-quantum (DQ) or a zero-quantum (ZQ) transition (Fig. 1A). Although these transitions are formally forbidden, they become weakly allowed because of the mixing of nuclear Zeeman eigenstates via the $\hat{S}_z\hat{I}^{\pm}$ terms in the dipole Hamiltonian as illustrated in Fig. 1 (*9*–*13*). In 1976, there was a cursory mention by de Boer *et al.* (*14*, *15*) of the observation of a higher-order SE in ^{2}H spectra recorded at 0.7 K and 2.5 T with an enhancement of ~3 at twice the nuclear Larmor frequency ($\Omega_S = \pm 2\omega_{0I}$). Although the effect was not analyzed, it was suggested to be due to a three-spin system composed of an electron and two nuclei, i.e., TSSE. Similarly, the matching conditions at ($\Omega_S = \pm 2\omega_{0I}$) are attributed to the excitation of the single-quantum (SQ) or triple-quantum (TQ) transition (Fig. 1A) present in the three-spin system. The weak enhancement ε observed was not surprising given that the forbidden transitions exploited at the normal SE condition are only weakly allowed, and thus, exciting the highly forbidden TSSE transition is expected to be more challenging. More recently, Smith *et al.* (*16*) attempted to reinvestigate the TSSE, but the enhancement was not directly observable. In addition, a similar multinuclear effect, ^{1}H-^{13}C heteronuclear CE, was demonstrated at 3.4 T and 6.5 K (*17*). However, the actual enhancement factor was not reported because of the inability to observe the thermal equilibrium signal. Here, we report an enhancement factor ε ~ 170 (vide infra) at the TSSE conditions using trityl radical dispersed in a glassy glycerol-water matrix at 0.35 T and 80 K. To our knowledge, this is the largest enhancement ever observed for such an effect. We have analyzed the TSSE theoretically and by numerical simulations, which show that the effect is very sensitive to the electron-nuclear distances *r*. Hence, we exploit this feature to probe the structure and chemical environment around the radical and to provide insight into the DNP polarization pathway involving the spin diffusion mechanism (*3*, *18*).

As mentioned earlier, the spin diffusion process plays an essential role in transferring the polarization from the DNP-enhanced near nuclei to the bulk nuclei. However, the nuclei neighboring the polarizing agent are generally thought to experience a large local field originating from the hyperfine interaction, and this induces a shift in the precession frequency away from the bulk resonances and thereby quenches the spin diffusion mechanism. Moreover, the random modulation of the hyperfine interactions could lead to fast relaxation rates for the near nuclei and hence relaxes the hyperpolarized signal. The

[1]Francis Bitter Magnet Laboratory and Department of Chemistry, Massachusetts Institute of Technology, Cambridge, MA 02139, USA. [2]Department of Electrical Engineering, Technical University of Denmark, Kgs. Lyngby 2800, Denmark. [3]GE Healthcare, Brøndby 2605, Denmark.
*Present address: Aspen Technology Inc., 20 Crosby Drive, Bedford, MA 01730, USA.
†Corresponding author. Email: rgg@mit.edu

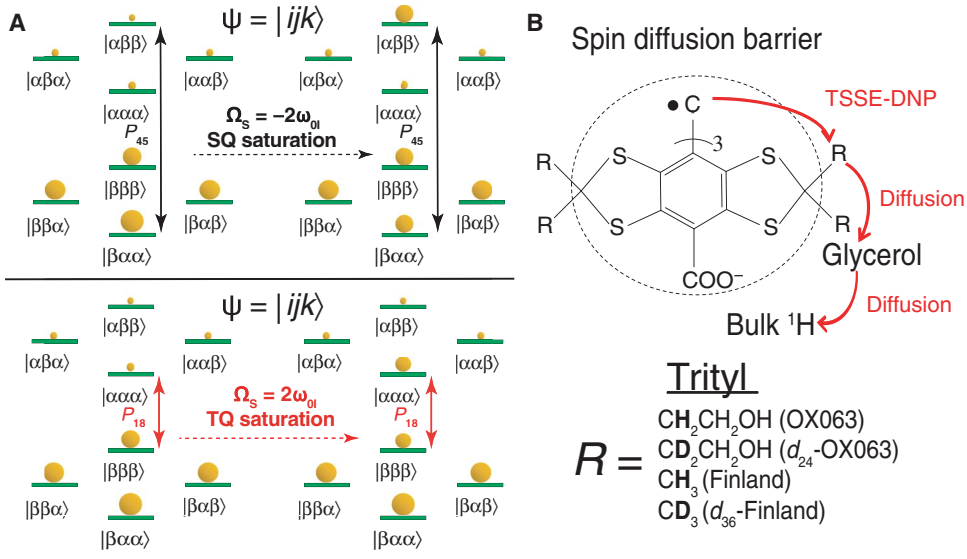

Fig. 1. Schematic diagram of an energy-level diagram and a spin diffusion barrier. (**A**) Energy level diagram of a three-spin system showing the highly forbidden [SQ (top) and TQ (bottom)] transitions that mediate TSSE-DNP. (**B**) Schematic diagram of the spin diffusion barrier and trityl radicals.

near nuclei in this regime are often referred to as the "core" nuclei, which reside within the spin diffusion barrier (Fig. 1B) (*19*–*21*), and their polarization has a limited contribution to the bulk signal. There have been several attempts to quantify the size of this barrier with examples of low-temperature studies of single crystals doped with paramagnetic ions (*20*, *22*); however, a broad range of values ranging from 3 to 17 Å are reported in the literature (*20*, *22*–*28*). Given the ongoing renaissance in DNP using bulky organic radicals in amorphous glassy matrices, as opposed to paramagnetic metal ions in single crystals, it is important to determine the size of the spin diffusion barrier on an amorphous frozen solution such as OX063 in glycerol/water. In this contribution, using several independent approaches such as using trityl radicals with deuterated side chains and solvents with various degree of deuteration, we show that the limit on the size of the spin diffusion barrier is <6 Å for trityl radical in an amorphous glycerol-water matrix. Furthermore, a comparison of ^{1}H ENDOR spectra of ^{2}H and ^{1}H glycerol reveals that the trityl radicals form a cluster with the glycerol molecules, shielding themselves from the water molecules. Thus, the initial step in the polarization transfer is to ^{1}H's on glycerol. These results provide important information on the spin diffusion pathway and aid the design of DNP polarizing agents for applications in a number of different areas.

Theory

We consider a three-spin e^{-}-^{1}H-^{1}H system ($\psi = |ijk\rangle$), where the quantum numbers i, j, and k refer to the spin states of the electron, nucleus 1, and nucleus 2, respectively. The general Hamiltonian of such a system in the electron rotating frame is given by

$$\hat{\mathcal{H}} = \Omega_S\hat{S}_z - \omega_{0I}(\hat{I}_{1z} + \hat{I}_{2z}) + \hat{S}_z(A_1\hat{I}_{1z} + A_2\hat{I}_{2z}) + \hat{S}_z(B_1\hat{I}_{1x} + B_2\hat{I}_{2x}) \quad (1)$$

where A and B are the secular and nonsecular components of the hyperfine interaction, respectively, and Ω_S is the microwave offset frequency. The Hamiltonian $\hat{\mathcal{H}}$ can be transformed to a diagonalized form $\hat{\mathcal{H}}^{\Lambda}$

$$\hat{\mathcal{H}}^{\Lambda} = \hat{U}\hat{\mathcal{H}}\hat{U}^{-1}$$
$$\hat{U} = \exp\left(-i\sum_{k=1,2}(\eta_{k\alpha}\hat{S}_\alpha\hat{I}_{ky} + \eta_{k\beta}\hat{S}_\beta\hat{I}_{ky})\right) \quad (2)$$

where the operators $\hat{S}_{\alpha/\beta}$ and angles $\eta_{k\alpha/k\beta}$ are given by

$$\hat{S}_\alpha = \frac{\hat{1}}{2} + \hat{S}_z;\quad \hat{S}_\beta = \frac{\hat{1}}{2} - \hat{S}_z$$
$$\eta_{k\alpha} = \tan^{-1}\frac{-B_k}{A_k - 2\omega_{0I}};\ \eta_{k\beta} = \tan^{-1}\frac{-B_k}{A_k + 2\omega_{0I}} \quad (3)$$

where $\hat{1}$ represents the identity operator. Following that, the eigenvalues and henceforth the matching conditions for the SQ $|\alpha\beta\beta^{\Lambda}\rangle \leftrightarrow |\beta\alpha\alpha^{\Lambda}\rangle$ and TQ $|\alpha\alpha\alpha^{\Lambda}\rangle \leftrightarrow |\beta\beta\beta^{\Lambda}\rangle$ transitions, which are responsible for the TSSE, can be determined from the diagonalized Hamiltonian $\hat{\mathcal{H}}^{\Lambda}$ (Eq. 2) using Mathematica (Wolfram Research)

$$\Omega_S = \pm\sum_{k=1,2}\left(\sqrt{B_k^2 + (A_k + 2\omega_{0I})^2} + \sqrt{B_k^2 + (A_k - 2\omega_{0I})^2}\right)/4$$
$$\sim\pm 2\omega_{0I} \text{ if } A_k, B_k \ll \omega_{0I} \quad (4)$$

Following that, the transition amplitudes of the TQ and SQ transitions (see the Supplementary Materials for details of the derivation) are given by

$$a_{ij} = \langle\psi_i^{\Lambda}|\,\hat{U}\omega_{1S}\hat{S}_x\,\hat{U}^{-1}\,|\psi_j^{\Lambda}\rangle$$
$$a_{18} = a_{45} = \frac{-\omega_{1S}}{8}\left(e^{i(\eta_{1\alpha}+\eta_{1\beta}+\eta_{2\alpha}+\eta_{2\beta})/2}\right)\left(e^{-i\eta_{1\alpha}} - e^{-i\eta_{1\beta}}\right)\left(e^{-i\eta_{2\alpha}} - e^{-i\eta_{2\beta}}\right)$$
$$\approx\frac{B_1B_2\omega_{1S}}{8\omega_{0I}^2} \text{ if } A_k, B_k \ll \omega_{0I} \text{ and } \omega_{1S} \ll \omega_{0I} \quad (5)$$

where $|\psi^{\Lambda}\rangle$ are the eigenstates in $\hat{\mathcal{H}}^{\Lambda}$. Typically, $A_k/2\pi$, $B_k/2\pi$, and $\omega_{1S}/2\pi \sim 1$ MHz and $\omega_{0I}/2\pi \sim 15$ MHz, so the inequalities are satisfied. Note that the TSSE transition amplitudes (Eq. 5) are proportional to B^2 or r^{-6}, where r is the electron-nucleus distance assuming $B_1 = B_2$. Moreover, the transition amplitudes $a_{18}(a_{45})$ (Eq. 5) show that the highly forbidden TQ (SQ) transitions depend on the product of the two electron-nucleus dipolar couplings and that the nuclear-nuclear coupling is not required, as confirmed by numerical simulations. Similarly, the transition amplitudes of a normal two-spin SE can be derived from $\hat{\mathcal{H}}^{\Lambda}$ (Eq. 2) and shown to be

$$a_{35} = -a_{17} = \frac{B\omega_{1S}}{4\omega_{0I}} \tag{6}$$

which, assuming $B_1 = B_2$, is ~$2\omega_{0I}/B$ times larger than those of the TSSE (Eq. 5). Following that, the transition probabilities can be determined by applying Fermi's golden rule

$$P_{ij} = |a_{ij}|^2$$

$$P_{17} = P_{35} = \frac{B^2\omega_{1S}^2}{16\omega_{0I}^2}$$

$$P_{18} = P_{45} = \frac{B_1^2 B_2^2 \omega_{1S}^2}{64\omega_{0I}^4} \tag{7}$$

which yields the well-known result that the transition probability of the SE P_{17} (or P_{35}) is proportional to ω_{0I}^{-2}. Note that the TSSE transition probability P_{18} (or P_{45}) has a field dependence of ω_{0I}^{-4}. Thus, it is not surprising that the TSSE enhancement is small or not easily observable at higher fields (*15*, *16*). Further discussion on the relevance of Fermi's golden rule, Rabi frequency ω_{1S}, and relaxation effect on the DNP enhancement can be found in the literature for interested readers (*10*).

RESULTS AND DISCUSSION

The field profiles in Fig. 2A show that the bulk ^{1}H nuclei are hyperpolarized at the SE and TSSE conditions at $\Omega_S = \pm 15$ MHz and $\Omega_S = \pm 30$ MHz, respectively. The experimental observations agree well with the predicted matching conditions (Eq. 4) and the energy level diagram (Fig. 1A). The enhancement factors are $\varepsilon \sim \pm 220$ for OX063 trityl at the SE conditions and $\varepsilon \sim \pm 100$ for the TSSE, using a Rabi frequency of $\omega_{1S}/2\pi = 2$ MHz and a polarization time of $\tau = 8$ s (see fig. S1). The TSSE enhancement can be further optimized to obtain $\varepsilon \sim 170$ (vide infra) by using a longer τ and higher ω_{1S}.

Effect of solvent deuteration on the TSSE

The theoretical analysis of the TSSE implies that the enhancement factor is sensitive to the electron-nuclei distance r, and this has enabled us to examine the DNP polarization pathway from the radical to the bulk ^{1}H nuclei. Before directly investigating that issue, it is important to justify that the ^{1}H's involved in the TSSE originate from the intramolecular protons on the radical, as opposed to the solvent. We recorded field profiles using similar conditions but with solvents of different ^{1}H concentrations (Fig. 2B), i.e., double or half of the H_2O volume ratio in "DNP juice" (d_8-glycerol:D_2O:H_2O, 60:30:10 by volume). In principle, altering the ^{1}H concentration directly influences the DNP enhancement because it changes the average number of

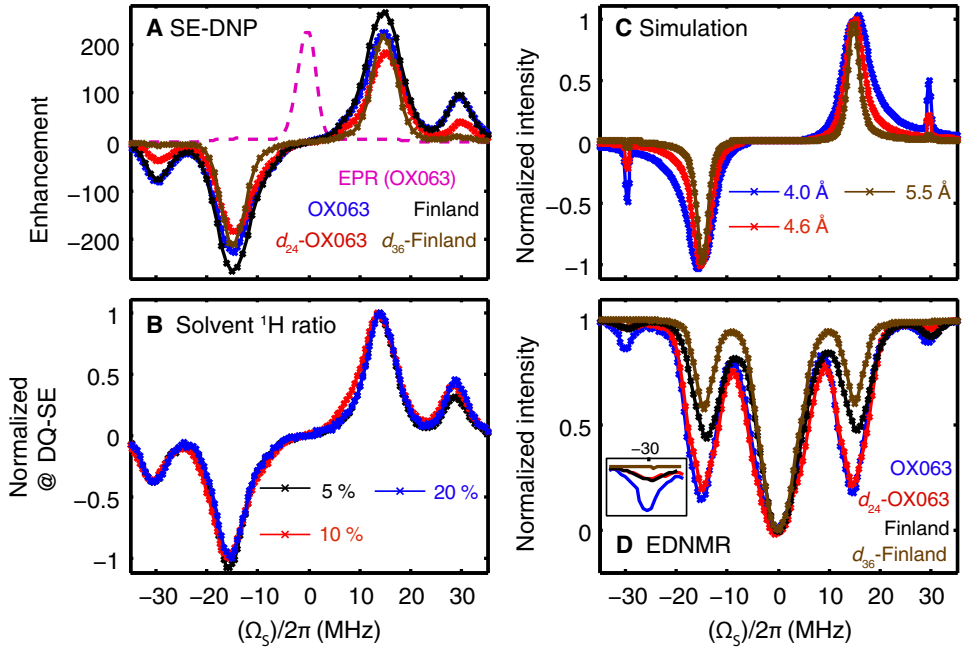

Fig. 2. EPR spectrum, DNP field profiles, and EDNMR spectra at 0.35 T. SE-DNP field profiles (**A** to **C**) for (A) various trityl radicals, (B) trityl OX063 with solvents of different H_2O ratios, and (C) simulations with different distances r_{eff}. An electron paramagnetic resonance (EPR) spectrum of OX063 (magenta) is also shown in (A) as a reference. The other trityl radicals have similar spectra and therefore are not shown. The field profiles in (B) are all normalized with the enhancement obtained at the DQ-SE ($\Omega_S = -15$ MHz) condition. (**D**) Normalized ELDOR (electron-electron double resonance)–detected NMR (EDNMR) spectra with an inset in an expanded view were acquired using a saturating pulse of 3 ms. All field profiles were obtained by changing the microwave frequency while keeping the magnetic field constant, which could explain the slight asymmetry observed in the field profiles, as the Rabi frequency might be different at different microwave frequencies.

^{1}H nuclei polarized per radical and the mean ^{1}H-^{1}H distance, which affects the spin diffusion rate. Nevertheless, we expect that these two factors will affect both the SE and TSSE enhancements in the same manner, and hence, we normalize the enhancement at the DQ-SE (Ω_S = 15 MHz) condition to unity in each field profile (Fig. 2B). If the efficiency of the normal SE depends on the probability p of finding one proton to be within a certain radius surrounding the radical, then the TSSE's efficiency will be proportional to p^2 accordingly as two protons are required. Thus, if the TSSE is mediated via the solvent protons, then we expect the TSSE enhancements to be higher (lower) when the ^{1}H content of the solvent is higher (lower). The fact that the normalized field profiles in Fig. 2B are not altered by changing the ^{1}H concentration of the solvent implies that the TSSE is not mediated by solvent but rather by the intramolecular ^{1}H's in the radical.

Effect of deuterating the trityl radicals on the TSSE

To further support our assertion that the TSSE is mediated via the intramolecular protons, we repeated the experiments on various trityl radicals (Fig. 1B) under the same conditions. The experimental results show that the TSSE enhancements decrease by ~50% (Fig. 2A) when the closest 24 methylene –CH_2 groups in OX063 are deuterated, while the change in normal SE enhancements is smaller, i.e., 18% drop in ε. We presume that the TSSE enhancements are not fully suppressed because of the remaining protonated methylene groups farther from the electron. On the other hand, similar experiments performed on the Finland trityl show that the TSSE ε quenched by ~90%, i.e., from ~100 to ~9 ± 3 (slightly above noise level) when perdeuterated d_{36}-Finland is used. Here, the absence of any remaining intramolecular protons renders the TSSE nearly unobservable. The experimental findings on these two different classes of radicals are in good agreement with our earlier assertion that the intramolecular protons are crucial in mediating the TSSE, whose transition amplitude has a ~B^2 dependence (Eq. 5) and therefore becomes inefficient if the closest protons are farther away (d_{24}-OX063 and d_{36}-Finland).

In addition, we performed numerical simulations on a simple three-spin model. To represent the large number of proton spins (up to 48 protons) on the radical with only two protons, we have adopted the notion of effective distance, r_{eff} (*29*–*31*), with values of r_{eff} = 3.8, 4.4, and 5.5 Å to model the OX063, d_{24}-OX063, and d_{36}-Finland trityl radicals, respectively. We neglected the protonated Finland trityl in the simulations because the methyl group dynamics might affect the DNP enhancement and are ill posed in our simplified description. The value of r_{eff} for the d_{36}-Finland was adopted from the estimated distances of the solvent protons (*31*, *32*), while the justification of other r_{eff} values was explained in the numerical simulation section (vide supra). The numerical results (Fig. 2C) show that ε is in fact more sensitive to r_{eff} in the TSSE than in the normal SE, i.e., ε at Ω_S ~ ±30 MHz is attenuated by ~50 and 90% (Table 1) when the value of r_{eff} increases from 3.8 Å to 4.4 and 5.5 Å, respectively. We note that the TSSE lines are narrower in the simulation than in the experimental data, and it could be that a three-spin system is insufficient to fully represent a trityl molecule, i.e., more protons with a distribution of hyperfine couplings are required. Another consideration is that the relaxation parameters of the nuclei (T_{1n} and T_{2n}) might not be the same for all nuclei, and there might be a distribution of values for these parameters depending on their distances from the electron. These effects are, however, difficult to incorporate into numerical simulations.

The good agreement between numerical simulations, experimental results, and analytical theory supports our hypothesis that the polarization in the TSSE is mediated via the protons on the radical, which then contributed to the observed bulk ^{1}H signal via spin diffusion. In other words, the intramolecular protons, such as the methylene –CH_2 groups in OX063 or the methyl –CH_3 groups in Finland trityl radical, must be outside the spin diffusion barrier or else we would not be able to enhance the polarization of the bulk protons at the TSSE conditions. As the average distances of the methyl protons are reported to be 5.6 ± 0.2 Å (*31*) and the methylene protons are ~6.0 Å [from the density functional theory (DFT) calculations explained in the Supplementary Materials], we conclude that the radius of the spin diffusion barrier is <6 Å. This result is in good agreement with the size of a spin diffusion barrier surrounding the vanadyl complex, which was found to be between 4 and 6.6 Å using electron paramagnetic resonance (EPR) spectroscopy (*28*).

ENDOR and EDNMR studies of the trityl radical

In principle, it is possible for the nearest solvent ^{1}H from glycerol or H_2O to have shorter electron-nuclear distances than the intramolecular ^{1}H's alluded to above, and these ^{1}H's could contribute substantially to the TSSE-DNP. To examine this possibility, we performed ^{1}H ENDOR experiments (Fig. 3) using d_{36}-Finland trityl in glycerol/H_2O/D_2O mixtures to investigate this possibility for our experiments performed in DNP juice (*31*, *32*). The result shows that the full width at half maximum of the ^{1}H ENDOR lines acquired using h_8-glycerol/H_2O and h_8-glycerol/D_2O mixtures is about twice as broad as the d_8-glycerol mixture (DNP juice), indicating that the –CH_2 groups in the glycerol molecule are more strongly coupled to the electron than the water molecule. This experimental observation suggests that the glycerol molecules in the solvent are shielding the trityl radical from the water molecules, thereby causing the direct polarization of water ^{1}H's in the DNP juice to be less efficient.

The ENDOR spectrum also permits to estimate the distance between the radical and the solvent ^{1}H's. Note that the ENDOR spectra acquired are featureless, i.e., no distinct Pake doublets that can be identified easily. Nevertheless, the foot of the spectra (at ~1% intensity of the normalized spectrum) possibly corresponds to the largest

Table 1. Values of the parameter r_{eff} used and the enhancements factors extracted from Fig. 4. The renormalized ε_{TSSE} values reported are normalized with respect to the values obtained for OX063 in the first column.

	OX063	d_{24}-OX063	d_{36}-Finland
$\langle R \rangle$ (Å)	5.98	6.96	5.5
N	24	24	2
r_{eff} (Å)	3.96	4.6	5.5
Actual expt ε_{TSSE}	93	40	11
Expt ε_{TSSE} (renormalized)	93/93 = 1	40/93 ~ 0.43	11/93 ~ 0.12
Normalized sim ε_{TSSE}	0.498	0.218	0.059
Sim ε_{TSSE} (renormalized)	0.498/ 0.498 = 1	0.218/0.498 ~ 0.44	0.059/0.498 ~ 0.12

splitting, and this value is assigned to the parallel principal value of a purely dipolar interaction between the proximate solvent ^{1}H and the radical. For the case of DNP juice, the full breadth of the extreme ends of the ENDOR line is ~0.9 MHz, which yields an estimated lower limit of the e^--^{1}H distance to be ~5.6 Å. Note that this is a qualitative analysis and resembles only a tiny fraction of the solvent ^{1}H's close to the electron. The result shows that, in the optimal (but unlikely) scenario, most solvent protons are farther away from the radical than the electron-CH_3 distances. The results agree well with our hypothesis that the intramolecular protons on the radical are the main contributors to the TSSE. Besides that finding, the weak hyperfine interaction observed between the water molecules and the electron also explains the similar field profiles when the solvent ^{1}H ratio is altered (Fig. 2B).

Note that we have only quoted an upper limit for the size of the barrier. To more accurately probe the size of the barrier, i.e., determining the lower limit, one would need to synthesize an array of stable radicals with different electron-nuclear distances with an option of ^{2}H isotope labeling. The approach is beyond the scope of this work. Moreover, the spin diffusion barrier is merely a classical model. In reality, the barrier should be orientation dependent rather than spherical because of the anisotropic nature of dipolar couplings (*19*). Last, the rate of spin diffusion should experience a gradual change near the barrier rather than an abrupt jump as proposed in the model.

In addition, we have also performed the ELDOR (electron-electron double resonance)–detected NMR (EDNMR) (*33*) experiments (Fig. 2D) to cross-verify the DNP field profiles. The experiment is similar to SE-DNP except that the electron polarization signal is monitored instead of the bulk ^{1}H. Since the total polarization is conserved, the gain in NMR polarization in SE-DNP must originate from the loss of electron polarization (*16*). Thus, the loss of electron polarization due to saturation of the forbidden transitions can provide complementary information to the DNP efficiency. For instance, we observed $\varepsilon \sim 93$, 94, 40, and 11 in DNP (Fig. 2A) for the OX063, Finland, d_{24}-OX063, and perdeuterated d_{36}-Finland trityls, respectively. These enhancement numbers in ratio, i.e., 93:94:40:11 or approximately 9:9:4:1, correlate well to the ~11, 8, 5, and 1% of the electron polarization attenuated at Ω_S = 30 MHz in EDNMR. Another advantage of performing EDNMR experiment is that it can be used to detect the presence of nearby nuclei within the spin diffusion barrier, which act as a sink for electron polarization. These nearby nuclei are, however, not easily observable in the DNP experiment. Nevertheless, we notice that the saturation factor at $\Omega_S = \pm 15$ MHz has little relevance to the SE ε, and it is likely that the microwave field is reaching a regime where the nearby nuclei are polarized by DNP more rapidly than the bulk nuclei are polarized by spin diffusion (vide infra).

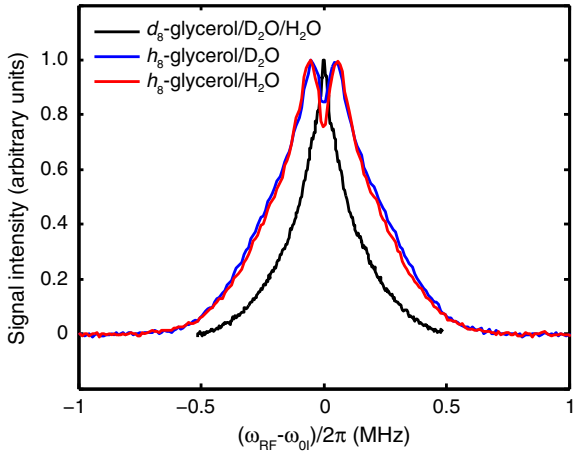

Fig. 3. ^{1}H ENDOR spectra using different solvent conditions at 0.35 T. Normalized ^{1}H ENDOR spectra at 80 K recorded on 0.5 mM d_{36}-Finland trityl in 60:40 by volume glycerol/water mixtures, with either deuterated or protonated components. The mixtures are "DNP juice" (d_8-glycerol:D_2O:H_2O, 60:30:10 by volume; black), ^{1}H glycerol with 99.9% D_2O (blue), or 99.9% H_2O (red).

Buildup curve and power dependence of the TSSE

We emphasize that the transition probability P_{ij} directly influences, but does not dictate, the nominal enhancement factor. In particular, a similar enhancement factor can be achieved by exploiting a longer mixing time for experiments using a weaker ω_{1S} in near-ideal cases (*34*, *35*), for instance, when the DNP mechanism is sufficiently efficient relative to the rate of spin diffusion and the relaxation constants. This is supported by the measured enhancements of $\varepsilon \sim 175$ to 250 (*36*) obtained using the NOVEL (nuclear orientation via electron spin locking) sequence, which theoretically has a higher transition probability but similar ε compared to SE. Figure 4 shows the dependence of the enhancement ε on the Rabi frequency ω_{1S} and the mixing time τ. At $\omega_{1S}/2\pi \sim 0.2$ MHz, the ratio of the enhancement from the TSSE to the two-spin SE condition is only $\varepsilon_{TSSE}/\varepsilon_{SE} = 17/185 \sim 0.09$ and continues to increase as ω_{1S} increases. This is as expected since a larger ω_{1S} is required to saturate the highly forbidden TSSE condition. Both enhancement factors begin to saturate at ~2 MHz, and the ratio becomes $\varepsilon_{TSSE}/\varepsilon_{SE} = 168/284 \sim 0.6$, which is evidently higher than $P_{18}/P_{14} = (B^2)/(4\omega_{0I}^2) \sim 10^{-3}$ (Eq. 7). This shows that the concept of directly correlating transition probability P_{ij} to the actual enhancement ε, as it is usually adopted in the literature, does not necessarily suffice in all cases. Nevertheless, one can show theoretically that this notion is applicable in characterizing the initial polarization buildup at a short time t such that $\sqrt{P_{ij}}t \ll 1$. We believe that the ratio $\varepsilon_{TSSE}/\varepsilon_{SE}$ reaches only 0.6 instead of unity because it is still fundamentally limited by the proton relaxation rate. The polarization buildup curve (Fig. 4B) shows that the increments in the DNP enhancement for both conditions are marginal past $T_{1n} \sim 13$ s. The results shown here have important implications to the observation of TSSE at higher fields (*16*), which was deemed difficult because of the unfavorable scaling of $P_{TSSE} \sim \omega_{0I}^{-4}$ (Eq. 7). Nevertheless, we hypothesize that moderate

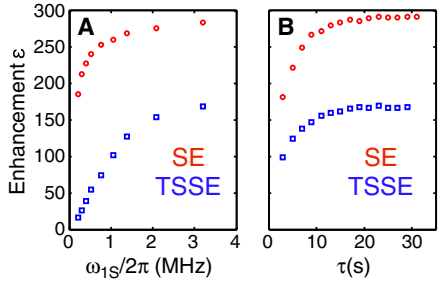

Fig. 4. Power dependence and buildup curves for SE and TSSE. Enhancement ε as a function of the (**A**) Rabi frequency $\omega_{1S}/(2\pi)$ with a fixed time $\tau \sim 24$ s and (**B**) time τ with a fixed $\omega_{1S}/(2\pi) \sim 3.2$ MHz. The microwave cavity is critically coupled in these experiments to obtain a high *Q* factor and hence Rabi frequency at a fixed microwave frequency of 9.801 GHz. The data are recorded at the field position that corresponds to either ZQ-SE (red) or SQ-TSSE (blue).

enhancement can be achieved by exploiting higher nutation frequency ω_{1S} and/or lower temperatures (*14*, *15*).

MATERIALS AND METHODS

Sample preparation

We performed DNP and EPR studies on four different trityl radicals, namely, OX063, deuterated d_{24}-OX063, Finland (*37*), and perdeuterated d_{36}-Finland (Fig. 1B). The trityl radicals were obtained from GE Healthcare (Amersham, UK). Samples of 5 mM trityl dispersed in a mixture of d_8-glycerol:D_2O:H_2O (60:30:10 by volume), also known as DNP juice, were used in all DNP experiments except for the dilution analysis (Fig. 2B).

DNP-NMR and EPR spectroscopy

Using instrumentation similar to that described previously (*35*, *38*, *39*), we performed all experiments at a temperature of T = 80 K and B_0 = 0.35 T. The presaturation of the ^{1}H channel (fig. S1) was performed before the DNP sequence to suppress the remaining NMR polarization. This was achieved using eight 30° pulses spaced by a delay of 100 μs. The ^{1}H echo signal was generated using solid echo with delays of 20 μs, so that the signal remains detectable beyond the receiver dead time and avoids the distortion by the ringdown in the probe. The ^{1}H thermal equilibrium polarization was measured using the same sequence, with microwaves turned off and $\tau \sim 3T_{1n}$. We defined the enhancement factor as the integrated ^{1}H signal intensity, with microwaves turned on, scaled with the same integrated signal without microwave irradiation at full ^{1}H thermal equilibrium, extrapolated from the measured signal at $\sim 3T_{1n}$. The EPR spectra were obtained by using spin echo–detected spectra in a field-swept experiment. The Mims ENDOR experiments, i.e., [$\pi/2 - d - \pi/2$ – RF (T_{RF}) – $\pi/2 - d$ – echo], were performed using a Bruker DICE-II ENDOR system with a 250-W radio frequency (RF) amplifier. The delay d = 300 ns was chosen so that the blind spots occur at integer multiples of $1/d \sim 3.33$ MHz, which are much larger than the largest hyperfine coupling expected in trityl. RF pulses (25 W) and T_{RF} = 160 μs were used to excite the allowed NMR transitions. The RF sweep was performed using a stochastic mode. The EDNMR experiments were performed with a high-turning angle pulse of 3 ms with a Rabi frequency of 2 MHz at 80 K.

Numerical simulations

The numerical simulations were performed using a custom-built simulation package (*40*) written in MATLAB (MathWorks). Relaxation effect was incorporated in the program using relaxation superoperators in Liouville space (*41*). Relaxation times of T_{1e} = 0.6 ms and T_{2e} = 5 μs for the electron and of T_{1n} = 13 s and T_{2n} = 1 ms for both ^{1}H nuclei were used in the simulations. We used $\omega_{1S/2\pi}$ = 2 MHz, τ = 16 ms, and 100 different powder orientations chosen using the zero correlation window scheme in all simulations (*42*). Further details of the simulation package can be found in the Supplementary Materials and in our recently published work (*40*). We determined the effective electron-nuclei distance by computing $r_{eff} = (N/2)^{1/6}\langle R\rangle$ (Table 1), where $\langle R\rangle$ is the average electron-nuclei distances of the closest nuclei in the first shell considered for our simulation and N is the number of nuclei. Note that the factor 2 was included because two protons were considered in the numerical simulations. The values of $\langle R\rangle$ for the OX063 radical were determined from the DFT calculations (see the Supplementary Materials), and we used an intermediate value of 5.5 Å for the case of solvent protons (for d_{36}-Finland), which were reported to be in the range of 4.8 to 5.8 Å away from the radical (*31*, *32*, *43*).

CONCLUSION AND OUTLOOK

We have demonstrated in this article the observation of an enhancement ε = 170 for the TSSE for the trityl radical at 0.35 T and 80 K, which is the largest value reported to date for this effect. The experimental results are consistent with the theoretical analysis and numerical simulations, i.e., a three-spin electron-nuclei-nuclei system is required to explain the experimental observation. Furthermore, the fact that the transition amplitude of the TSSE is proportional to r^{-6} allows us to use it as a tool to provide structural information of the radical, as well as the spin diffusion pathway during the DNP process. For instance, our study showed that the TSSE-DNP is mediated via the intramolecular ^{1}H rather than the solvent ^{1}H. Following that result, it permits us to probe the size of the spin diffusion barrier, which arises because of strong hyperfine interactions with the nearby nuclei. Our results have shown that the size of the barrier is <6.0 Å for the important organic radical trityl in a glycerol-water matrix. This represents the first measurement of the size of the spin diffusion barrier for a bulky organic radical in amorphous solids. In addition, the ^{1}H ENDOR spectra are consistent with the idea that the glycerol molecules are in close proximity around the radical, shielding the hydrophobic part from the water molecules. Furthermore, this independent EPR data indirectly supports our results on the size of the spin diffusion barrier obtained with TSSE-DNP. By combining the results from ENDOR and TSSE-DNP, we are able to establish the DNP polarization pathways starting from the unpaired electron to the bulk nuclei. For this study on the trityl radicals in the glycerol/water mixture, the polarization from the unpaired electron is transferred first to the intramolecular ^{1}H via direct DNP (Fig. 1B) and then relayed to the bulk solvent via the glycerol molecules mediated by the spin diffusion mechanism. Our study has successfully elucidated one of the polarization transfer pathways in DNP. An understanding of the size of the spin diffusion barrier and the chemical environment surrounding the polarizing agent in amorphous matrices provides information to constrain the design of new radicals with optimized performance in DNP applications. For instance, the fact that there are no protons <6 Å distance from the central carbon atom (or within the spin diffusion barrier) of trityl, which could act like a polarization sink leading to inefficient DNP transfer, could explain why trityl is one of the more efficient DNP polarizing agents. Last, we note that, among the stable free radicals currently in use as polarizing agents, trityl is unique in that the electron is largely localized (spin density ~ 0.75) (*32*) on the central carbon atom. This is in contrast to 1,3-bis(diphenylene)-2-phenylallyl (BDPA), where the TSSE was first observed, and the electron is delocalized over the diphenylene rings. This results in large isotropic hyperfine interactions with nearby protons that are revealed by the EPR spectrum in a solution state (*44*). A third case is bis-nitroxides where the two unpaired electrons are localized on the N–O moieties. Thus, it is of interest to design experiments to examine the size of the diffusion barrier in these polarizing agents and to determine whether it is similar to or different from our current findings for the trityl radical.

SUPPLEMENTARY MATERIALS

Supplementary material for this article is available at http://advances.sciencemag.org/cgi/content/full/5/7/eaax2743/DC1

Section S1. Details of the simulation package

Section S2. DFT calculations on trityl OX063

REFERENCES AND NOTES

1. A. Abragam, M. Goldman, Principles of dynamic nuclear polarisation. *Rep. Prog. Phys.* **41**, 395–467 (1978).
2. T. R. Carver, C. P. Slichter, Polarization of nuclear spins in metals. *Phys. Rev.* **92**, 212–213 (1953).
3. N. Bloembergen, On the interaction of nuclear spins in a crystalline lattice. *Phys. Ther.* **15**, 386–426 (1949).
4. A. Abragam, W. G. Proctor, Une nouvelle methode de polarisation dynamique des noyaux atomiques dans les solides. *Comp. Rend. Acad. Sci.* **246**, 2253–2256 (1958).
5. A. W. Overhauser, Polarization of nuclei in metals. *Phys. Rev.* **92**, 411–415 (1953).
6. C. F. Hwang, D. A. Hill, New effect in dynamic polarization. *Phys. Rev. Lett.* **18**, 110–112 (1967).
7. M. Borghini, Spin-temperature model of nuclear dynamic polarization using free radicals. *Phys. Rev. Lett.* **20**, 419–421 (1968).
8. C. D. Jeffries, Polarization of nuclei by resonance saturation in paramagnetic crystals. *Phys. Rev.* **106**, 164–165 (1957).
9. Y. Hovav, A. Feintuch, S. Vega, Theoretical aspects of dynamic nuclear polarization in the solid state—The solid effect. *J. Magn. Reson.* **207**, 176–189 (2010).
10. K.-N. Hu, G. T. Debelouchina, A. A. Smith, R. G. Griffin, Quantum mechanical theory of dynamic nuclear polarization in solid dielectrics. *J. Chem. Phys.* **134**, 125105 (2011).
11. W. T. Wenckebach, The solid effect. *Appl. Magn. Reson.* **34**, 227–235 (2008).
12. K. R. Thurber, R. Tycko, Theory for cross effect dynamic nuclear polarization under magic-angle spinning in solid state nuclear magnetic resonance: The importance of level crossings. *J. Chem. Phys.* **137**, 084508 (2012).
13. B. Corzilius, A. A. Smith, R. G. Griffin, Solid effect in magic angle spinning dynamic nuclear polarization. *J. Chem. Phys.* **137**, 054201 (2012).
14. M. Borghini, W. de Boer, K. Morimoto, Nuclear dynamic polarization by resolved solid-state effect and thermal mixing with an electron spin-spin interaction reservoir. *Phys. Lett. A.* **48**, 244–246 (1974).
15. W. de Boer, Dynamic orientation of nuclei at low temperatures. *J. Low Temp. Phys.* **22**, 185–212 (1976).
16. A. A. Smith, B. Corzilius, O. Haze, T. M. Swager, R. G. Griffin, Observation of strongly forbidden solid effect dynamic nuclear polarization transitions via electron-electron double resonance detected NMR. *J. Chem. Phys.* **139**, 214201 (2013).
17. D. Shimon, Y. Hovav, I. Kaminker, A. Feintuch, D. Goldfarb, S. Vega, Simultaneous DNP enhancements of ^{1}H and ^{13}C nuclei: Theory and experiments. *Phys. Chem. Chem. Phys.* **17**, 11868–11883 (2015).
18. D. Suter, R. R. Ernst, Spin diffusion in resolved solid-state NMR spectra. *Phys. Rev. B.* **32**, 5608–5627 (1985).
19. J. P. Wolfe, Direct observation of a nuclear spin diffusion barrier. *Phys. Rev. Lett.* **31**, 907–910 (1973).
20. A. D. A. Hansen, J. P. Wolfe, Measurement of the nuclear spin diffusion barrier around Eu^{2+} ions in CaF_2. *Phys. Lett. A.* **66**, 320–322 (1978).
21. C. Ramanathan, Dynamic nuclear polarization and spin diffusion in nonconducting solids. *Appl. Magn. Reson.* **34**, 409–421 (2008).
22. A. R. King, J. P. Wolfe, R. L. Ballard, NMR of nuclei near a paramagnetic impurity in crystals. *Phys. Rev. Lett.* **28**, 1099–1102 (1972).
23. M. Goldman, Impurity-controlled nuclear relaxation. *Phys. Rev.* **138**, A1675–A1681 (1965).
24. J. Ramakrishna, F. N. H. Robinson, A transient effect in dynamic nuclear polarization. *Proc. Phys. Soc.* **87**, 945–951 (1966).
25. T. J. Schmugge, C. D. Jeffries, High dynamic polarization of protons. *Phys. Rev.* **138**, A1785–A1801 (1965).
26. J. P. Wolfe, R. S. Markiewicz, Near-nuclei magnetic resonance of CaF_2:Yb^{3+}. *Phys. Rev. Lett.* **30**, 1105–1107 (1973).
27. D. Tse, I. J. Lowe, Nuclear spin-lattice relaxation in CaF_2 crystals via paramagnetic centers. *Phys. Rev.* **166**, 292–302 (1968).
28. M. J. Graham, C.-J. Yu, M. D. Krzyaniak, M. R. Wasielewski, D. E. Freedman, Synthetic approach to determine the effect of nuclear spin distance on electronic spin decoherence. *J. Am. Chem. Soc.* **139**, 3196–3201 (2017).
29. G. T. Trammell, H. Zeldes, R. Livingston, Effect of environmental nuclei in electron spin resonance spectroscopy. *Phys. Rev.* **110**, 630–634 (1958).
30. M. Bowman, L. Kevan, R. N. Schwartz, Analysis of matrix nuclei spin flip satellite lines in EPR spectra: Application to trapped hydrogen atoms. *Chem. Phys. Lett.* **30**, 208–211 (1975).
31. S. N. Trukhan, V. F. Yudanov, V. M. Tormyshev, O. Y. Rogozhnikova, D. V. Trukhin, M. K. Bowman, M. D. Krzyaniak, H. Chen, O. N. Martyanov, Hyperfine interactions of narrow-line trityl radical with solvent molecules. *J. Magn. Reson.* **233**, 29–36 (2013).
32. M. K. Bowman, C. Mailer, H. J. Halpern, The solution conformation of triarylmethyl radicals. *J. Magn. Reson.* **172**, 254–267 (2005).
33. P. Schosseler, T. Wacker, A. Schweiger, Pulsed ELDOR detected NMR. *Chem. Phys. Lett.* **224**, 319–324 (1994).
34. T. V. Can, R. T. Weber, J. J. Walish, T. M. Swager, R. G. Griffin, Frequency-swept integrated solid effect. *Angew. Chem. Int. Ed. Engl.* **56**, 6744–6748 (2017).
35. S. K. Jain, G. Mathies, R. G. Griffin, Off-resonance NOVEL. *J. Chem. Phys.* **147**, 164201 (2017).
36. T. V. Can, R. T. Weber, J. J. Walish, T. M. Swager, R. G. Griffin, Ramped-amplitude NOVEL. *J. Chem. Phys.* **146**, 154204 (2017).
37. O. Y. Rogozhnikova, V. G. Vasiliev, T. I. Troitskaya, D. V. Trukhin, T. V. Mikhalina, H. J. Halpern, V. M. Tormyshev, Generation of trityl radicals by nucleophilic quenching of tris(2,3,5,6-tetrathiaaryl)methyl cations and practical and convenient large-scale synthesis of persistent tris(4-carboxy-2,3,5,6-tetrathiaaryl)methyl radical. *European J. Org. Chem.* **2013**, 3347–3355 (2013).
38. T. V. Can, J. J. Walish, T. M. Swager, R. G. Griffin, Time domain DNP with the NOVEL sequence. *J. Chem. Phys.* **143**, 054201 (2015).
39. G. Mathies, S. Jain, M. Reese, R. G. Griffin, Pulsed dynamic nuclear polarization with trityl radicals. *J. Phys. Chem. Lett.* **7**, 111–116 (2016).
40. K. O. Tan, C. Yang, R. T. Weber, G. Mathies, R. G. Griffin, Time-optimized pulsed dynamic nuclear polarization. *Sci. Adv.* **5**, eaav6909 (2019).
41. A. Karabanov, G. Kwiatkowski, W. Köckenberger, Spin dynamic simulations of solid effect DNP: The role of the relaxation superoperator. *Mol. Phys.* **112**, 1838–1854 (2014).
42. V. B. Cheng, H. H. Suzukawa, M. Wolfsberg, Investigations of a nonrandom numerical method for multidimensional integration. *J. Chem. Phys.* **59**, 3992–3999 (1973).
43. J. H. Ardenkjær-Larsen, B. Fridlund, A. Gram, G. Hansson, L. Hansson, M. H. Lerche, R. Servin, M. Thaning, K. Golman, Increase in signal-to-noise ratio of > 10,000 times in liquid-state NMR. *Proc. Natl. Acad. Sci. U.S.A.* **100**, 10158–10163 (2003).
44. T. V. Can, M. A. Caporini, F. Mentink-Vigier, B. Corzilius, J. J. Walish, M. Rosay, W. E. Maas, M. Baldus, S. Vega, T. M. Swager, R. G. Griffin, Overhauser effects in insulating solids. *J. Chem. Phys.* **141**, 064202 (2014).

Acknowledgments: We thank S. K. Jain, T. V. Can, A. Taguchi, and G. Mathies for stimulating discussion of the TSSE experiments and A. Thakkar for instrumentation support. Special thanks are accorded to M. Bowman for a thorough discussion of the ^{1}H ENDOR spectra. **Funding:** K.O.T. was supported by an Early Postdoc Mobility grant from the Swiss National Science Foundation (grant no. 165285). This research was supported by the National Institute of Biomedical Imaging and Bioengineering (EB002804 and EB002026) and the National Institute of General Medical Sciences (GM132997 and GM132079). **Author contributions:** K.O.T. designed and performed the experiments. K.O.T. carried out the theoretical analysis. K.O.T. and C.Y. ran the numerical simulations. M.M. performed the DFT calculations. J.H.A.-L. provided the sample materials. K.O.T. and R.G.G. wrote and edited the paper. **Competing interests:** The authors declare that they have no competing interests. **Data and materials availability:** All data needed to evaluate the conclusions in the paper are present in the paper and/or the Supplementary Materials. Additional data related to this paper may be requested from the authors.

Submitted 9 March 2019
Accepted 20 June 2019
Published 26 July 2019
10.1126/sciadv.aax2743

Citation: K. O. Tan, M. Mardini, C. Yang, J. H. Ardenkjær-Larsen, R. G. Griffin, Three-spin solid effect and the spin diffusion barrier in amorphous solids. *Sci. Adv.* **5**, eaax2743 (2019).